JPET Fast Forward. Published on March 23, 2021 as DOI: 10.1124/jpet.120.000166
This article has not been copyedited and formatted. The final version may differ from this version.

Title

Inhibition of G6PD activity attenuates right ventricle pressure and hypertrophy elicited by VEGFR inhibitor + hypoxia

Atsushi Kitagawa,[1] Christina Jacob,[1] Allan Jordan,[2] Ian Waddell,[2] Ivan F. McMurtry,[3] Sachin A Gupte[1*]

[1]Department of Pharmacology, New York Medical College, Valhalla, NY

[2]Drug Discovery Unit, Cancer Research UK Manchester Institute, University of Manchester, Macclesfield, SK10 4TG, U.K.

[5]Departments of Pharmacology and Internal Medicine and Center for Lung Biology, College of Medicine, University of South Alabama, Mobile, AL

***Address Correspondence to**: Sachin A Gupte, MD, PhD, Professor of Pharmacology, New York Medical College, BSB 546, 15 Dana Road, Valhalla, NY 10595, Tel: 914-594-3937; email: sachin_gupte@yahoo.com or sgupte@nymc.edu

JPET Fast Forward. Published on March 23, 2021 as DOI: 10.1124/jpet.120.000166
This article has not been copyedited and formatted. The final version may differ from this version.

Running Title:

G6PD, DNA methylation, and PAH

Word Count:

Abstract: 241

Introduction: 462

Discussion: 1246

# of Figures: 5

# of Tables: 5

List of abbreviations:

DHEA: dehydroepiandrosterone
Dnmt: DNA methyltransferases
G6PD: glucose-6-phosphate dehydrogenase
Hx: hypoxia
IPA: solation of small intrapulmonary arteries
MTD: maximum tolerated dose
PASMC: pulmonary artery smooth muscle cell
PDD4091: N-[(3β,5α)-17-Oxoandrostan-3-yl]sulfamide
PH: Pulmonary hypertension
PPP: pentose phosphate pathway
RRBS: Reduced Representation Bisulfite Sequencing
RV: right ventricle
RVEDP: RV end-diastolic pressure
RVSP: RV systolic pressure
SMC: smooth muscle cell
SU: Sugen5416
Tet2: ten-eleven translocation 2

JPET Fast Forward. Published on March 23, 2021 as DOI: 10.1124/jpet.120.000166
This article has not been copyedited and formatted. The final version may differ from this version.

Abstract

Pulmonary hypertension (PH) is a disease of hyperplasia of pulmonary vascular cells. The pentose phosphate pathway (PPP) – a fundamental glucose metabolism pathway – is vital for cell growth. Because treatment for PH is inadequate, our goal was to determine whether inhibition of glucose-6-phosphate dehydrogenase (G6PD), the rate-limiting enzyme of the PPP, prevents maladaptive gene expression that promotes smooth muscle cell (SMC) growth, reduces pulmonary artery remodeling, and normalizes hemodynamics in experimental models of PH. PH was induced in mice by exposure to 10% oxygen (Hx) or weekly injection of vascular endothelial growth factor receptor blocker (Sugen5416 (SU); 20 $mg.kg^{-1}$) during exposure to hypoxia (Hx+SU). A novel G6PD inhibitor (N-[(3β,5α)-17-Oxoandrostan-3-yl]sulfamide;1.5 $mg\ kg^{-1}$) was injected daily during exposure to Hx. We measured right ventricle (RV) pressure and left ventricle (LV) pressure-volume relationships, and gene expression in lungs of normoxic, Hx, and Hx+SU, and G6PD inhibitor-treated, mice. RV systolic and end-diastolic pressures were higher in Hx and Hx+SU than normoxic-control mice. Hx and Hx+SU decreased expression of epigenetic modifiers (writers and erasers), increased hypomethylation of the DNA, and induced aberrant gene expression in lungs. G6PD inhibition decreased maladaptive expression of genes and SMC growth, reduced pulmonary vascular remodeling, and decreased right ventricle pressures, compared to untreated PH groups. Pharmacologic inhibition of G6PD activity, by normalizing activity of epigenetic modifiers and DNA methylation, efficaciously reduces RV pressure overload in Hx and Hx+SU mice, pre-clinical models of PH, appears to be a safe pharmacotherapeutic strategy.

Key Words: Pentose Phosphate Pathway; Mutations; Mediterranean; RNA-seq; DNA methylation; lungs; mice; rats; human.

JPET Fast Forward. Published on March 23, 2021 as DOI: 10.1124/jpet.120.000166
This article has not been copyedited and formatted. The final version may differ from this version.

Significance Statement: The results of this study demonstrated inhibition of a metabolic enzyme efficaciously reduces pulmonary hypertension. For first time, we show that a novel inhibitor of glucose-6-phosphate dehydrogenase, the rate-limiting enzyme in the fundamental pentose phosphate pathway, modulates DNA methylation and alleviates pulmonary artery remodeling and dilates pulmonary artery to reduce pulmonary hypertension.

JPET Fast Forward. Published on March 23, 2021 as DOI: 10.1124/jpet.120.000166
This article has not been copyedited and formatted. The final version may differ from this version.

Introduction

Pulmonary hypertension (PH) is a multifactorial disease that is defined as sustained elevation of pulmonary arterial pressure (Farber and Loscalzo, 2004). The elevation of pulmonary arterial pressure increases right ventricular (RV) afterload, leading to heart failure and death (Runo and Loyd, 2003). The main vascular changes in PH are vasoconstriction, vascular cell proliferation, and thrombosis. Based on these findings, current standard of care is treatment with vasodilators. However, vasodilators such as endothelin receptor blockers, nitric oxide/nitrates, prostacyclin, and phosphodiesterase-5 inhibitors, fail to reverse vascular remodeling, and the long-term prognosis remains poor (Lajoie et al., 2016).

Based on WHO classification PH is divided into five groups. WHO group 1 is pulmonary arterial hypertension; group 2 is PH from left-heart disease; group 3 is PH chronic from chronic hypoxic lung disease; group 4 is PH from chronic blood clots; and group 5 is PH from unclear multifactorial mechanisms (sarcoidosis, hematological disorders, etc). The pathogenesis of PH (Group 1 and Group 2) is still unclear. PH occurs under sustained environmental stress such as inflammation, shear stress, and hypoxia. This stress-stimuli contributes to the shifting of pulmonary vascular cells to hyper-proliferative and apoptotic-resistant phenotypes allowing abnormal vascular remodeling and PH development (Boucherat et al., 2017; D'Alessandro et al., 2018). Pulmonary vascular cells in patients with PH also undergo metabolic adaptation to support their high rate of proliferation or inadequate rates of mitotic fission. This metabolic shift, the Warburg phenomenon (Warburg et al., 1927), is a failure of mitochondrial respiration and activation of aerobic glycolysis.

The pentose phosphate pathway (PPP) – a branch of glycolysis and a fundamental glucose metabolism pathway – is vital for cell growth and survival. Glucose-6-phosphate

JPET Fast Forward. Published on March 23, 2021 as DOI: 10.1124/jpet.120.000166
This article has not been copyedited and formatted. The final version may differ from this version.

dehydrogenase (G6PD) is the first and rate-limiting enzyme of the PPP. G6PD and the PPP generate pentose sugar, which is required for the *de novo* cellular synthesis of RNA and DNA, and NADPH, a key cofactor for reductive and anabolic reactions. Recently, we found that inhibition and knockdown of G6PD in lungs of a chronic hypoxia-induced PH mouse model reduced and reversed: 1) Warburg phenomenon, 2) epigenetic modification (DNA methylation), 3) maladaptive expression of genes that support pulmonary artery remodeling, and 4) PH and left heart dysfunction (Joshi et al., 2020). However, the role of G6PD in the pathogenesis of hypoxia+Sugen5416–induced PH is unknown. Furthermore, whether inhibition of G6PD reduces remodeling of pulmonary artery and PH in hypoxia+Sugen5416 mouse model remains to be determined. We hypothesized that G6PD is a safe pharmacotherapeutic target to reduce PH in hypoxia+Sugen5416 mouse model. Therefore, our objectives were to determine whether the inhibition of G6PD activity by pharmacologic manipulations would decrease differential DNA methylation and maladaptive gene expression in lungs and pulmonary vascular cells, reduce vascular remodeling, and normalize hemodynamics in models of chronic hypoxia (Group 3)- and hypoxia+Sugen5416 (Group 1)-induced PH.

JPET Fast Forward. Published on March 23, 2021 as DOI: 10.1124/jpet.120.000166
This article has not been copyedited and formatted. The final version may differ from this version.

Materials and Methods

Drugs and reagents: All chemicals and reagents were purchased from Sigma, Thermo-Fisher, and VWR.

Animal models and experimental protocols: All animal experiments were approved by the New York Medical College Animal Care and Use Committee and all procedures conformed to the guidelines from the NIH Guide for the Care and Use of Laboratory Animals. Male and female C57BL/6J mice (18-32 g) were purchased from the Jackson Laboratory and randomly divided into four groups: normoxia (Nx), normoxia+Sugen5416 (Nx+SU), hypoxia (Hx), and hypoxia+Sugen5416 (Hx+SU) groups. Mice in Nx group were placed in normoxic (21% O_2) environment and in Hx group were placed in a normobaric hypoxic chamber (10% O_2) for 6 weeks (Joshi et al., 2020). Mice in Nx+SU and in Hx+SU group received subcutaneous injection of SU5416 (20 mg/kg) once weekly during 3 weeks of Nx (21% O_2) or Hx (10% O_2) as previously described (Vitali et al., 2014). Mice in the drug treatment groups received daily subcutaneous injection of a novel G6PD inhibitor, N-[(3β,5α)-17-Oxoandrostan-3-yl]sulfamide (PDD4091; 1.5 mg kg^{-1} day^{-1}) (Hamilton et al., 2012), for 3 weeks. To determine whether PDD4091 reduces PH in a dose-dependent manner, mice were randomized to receive low (0.15 mg kg^{-1} day^{-1}), medium (1.5 mg kg^{-1} day^{-1}), or high (15 mg kg^{-1} day^{-1}) dose injection of PDD4091. Hx and Hx+SU mice are pre-clinical models of PH (Stenmark et al., 2009). At the end of the treatment period, hemodynamic measurements were performed, tissue (lungs and arteries) were harvested, and blood samples were collected. Data analysis was performed in blinded fashion.

Hemodynamic measurements: All mice were anesthetized with inhalation of Isoflurane (isoflurane, USP; 1-chloro-2,2,2-trifluoroethyl difluoromethyl ether; induced at 3% and maintained at 1.5%) and placed on a heated table. Closed-chest cardiac catheterization was

JPET Fast Forward. Published on March 23, 2021 as DOI: 10.1124/jpet.120.000166
This article has not been copyedited and formatted. The final version may differ from this version.

performed using an MPVS Ultra Single Segment Pressure-Volume Unit (Millar Instruments, US) in combination with a cardiac catheter. RV systolic pressure (RVSP) and RV end-diastolic pressure (RVEDP) were measured by catheterization of the RV via the right external jugular vein using Millar Mikro-Tip catheter (model SPR-671, tip size of 1.4F, Millar Instruments, US). The catheter was then removed, and the jugular vein was tied off. For hemodynamic measurements from LV, the right carotid artery was dissected and a Millar Mikro-Tip conductance catheter (model SPR-839, tip size of 1.4F, Millar Instruments, US) introduced into the artery and advanced into the LV *via* the aortic valve. Once steady-state hemodynamics were achieved, pressure-volume (P-V) loops were recorded and analyzed using LabChart 8 software (ADInstruments, US).

Hematocrit measurements and blood chemistry analysis: After hemodynamic measurements were completed, blood was collected from the cardiac chambers into a heparinized syringe. Heparinized blood was placed in capillary tubes, and hematocrit (%) was calculated as the length of the erythrocyte layer divided by the length of the entire blood sample. Plasma was shipped to Antech Diagnostics (NC, USA), a GLP facility, where blood tests were performed with routinely used clinical laboratory diagnostic tools.

Assessment of right ventricular hypertrophy: Following the cardiac catheterization, the animals were euthanized by cervical dislocation and whole hearts were excised and RV free wall and LV including ventricular septum (S) were separated and weighed independently. Fulton's index (RV/LV + S ratio) was calculated as an index of RV hypertrophy.

Isolation of small intrapulmonary arteries (IPA) and IPA tone measurements: Mice (25-30g) were sacrificed by cervical dislocation and small intrapulmonary arteries (IPA) of 3rd order (100–150 μm in diameter) were isolated from the lung, dissected free of connective tissue, and placed in Krebs bicarbonate buffer solution (pH 7.4) containing the

JPET Fast Forward. Published on March 23, 2021 as DOI: 10.1124/jpet.120.000166
This article has not been copyedited and formatted. The final version may differ from this version.

following (in mM): 118 NaCl, 4.7 KCl, 1.5 $CaCl_2$ x$2H_2O$, 25 $NaHCO_3$, 1.1 $MgSO_4$, 1.2 KH_2PO_4, 5.6 glucose, and 10 HEPES. Then the vessels were mounted on a wire myograph (Danish Myo Technology A/S, Aarhus, Denmark) and bathed in Krebs buffer solution at 37°C and an optimal passive tension of 3 mN. After 30 min of incubation, the arterial viability and equilibration were assessed by the stimulation of the vessels with repeated 10 min exposures to KCl (60 mM; 60K). For registration of vascular ring contractile activity and its following analysis, Chart 5.5.4 and LabChart Reader 8.1.9 (ADInstruments, Inc.) software were used. Vascular tension is presented as a percentage of the maximum steady-state contraction level obtained to the exposure to 60K.

RNA-Seq analysis: After collecting lungs from Nx, Hx, and Hx+SU mice, total RNA was isolated from tissue using the Qiagen All Prep DNA/RNA/miRNA Universal kit according to manufacturer's instructions. RNA was quantified using the NanoDrop (ThermoFisher) and quality was assessed using the Agilent Bioanalyzer 2100. RNA-seq library construction was performed using the TruSeq Stranded Total RNA Preparation kit (Illumina) with 200 ng of RNA as input according to the manufacturer's instructions. Libraries were sequenced on the HiSeq2500 with single-end reads of 100nt at the University of Rochester Genomics Research Center. Single-end sequencing was done at a depth of 10 million reads per replicate. Quantitative analysis, including statistical analysis of differentially expressed genes, was done with Cufflinks 2.0.2 and Cuffdiff2 (http://cufflinks.cbcb.umd.edu). The Benjamini-Hochberg method was applied for multiple test correction (FDR<0.05).

Reduced Representation Bisulfite Sequencing (RRBS): To determine DNA methylation status in lungs of Nx, Hx, Hx+SU and Hx+4091 mice, genomic DNA was isolated from lungs using the Qiagen All Prep DNA/RNA/miRNA Universal kit according to manufacturer's instructions. DNA was quantified using the NanoDrop (ThermoFisher)

JPET Fast Forward. Published on March 23, 2021 as DOI: 10.1124/jpet.120.000166
This article has not been copyedited and formatted. The final version may differ from this version.

and Qubit Fluorometer (ThermoFisher). Genomic DNA quality was assessed using the Agilent TapeStation. RRBS library construction was performed with the Premium RRBS Kit (Diagenode) following the manufacturer's instructions. Libraries were sequenced on the HiSeq2500 with paired-end reads of 125nt. Raw reads generated from the Illumina HiSeq2500 sequencer were demultiplexed using bcl2fastq version 2.19.0. Quality filtering and adapter removal are performed using Trim Galore version 0.4.4_dev with the following parameters: " --paired --clip_R1 3 -- clip_R2 3 --three_prime_clip_R1 2 --three_prime_clip_R2 2" (http://www.bioinformatics.babraham.ac.uk/projects/trim_galore/). Processed and cleaned reads were then mapped to the mouse reference genome (mg38) using Bismark version 0.19.0 with the following parameters: " --bowtie2 --maxins 1000". Differential methylation analysis was performed using methylKit version 1.4.0 within an R version 3.4.1 environment. Bismark alignments were processed via methylKit in the CpG context with a minimum quality threshold of 10. Coverage was normalized after filtering for loci with a coverage of at least 5 reads and no more than the 99.9th percentile of coverage values. The coverage was then normalized across samples and the methylation counts were aggregated for 500nt windows spanning the entire genome. A unified window set across samples was derived such that only windows with coverage by at least one sample per group were retained. Differential methylation analysis between conditional groups was performed using the Chi-squared test and applying a qvalue (SLIM) threshold of 0.05 and a methylation difference threshold of 25 percent.

Quantitative real-time PCR: Real time RT-PCR technique was used to analyze mRNA expression. Briefly, total RNA was extracted from lungs using a Qiagen miRNEasy kit (Cat # 217004). The input RNA quality and concentration were measured on the Synergy HT Take3 Microplate Reader (BioTek, Winooski, VT) and cDNA was prepared using SuperScript IV. VILO Master Mix (Cat # 11756500, Invitrogen) for mRNA. Quantitative

JPET Fast Forward. Published on March 23, 2021 as DOI: 10.1124/jpet.120.000166
This article has not been copyedited and formatted. The final version may differ from this version.

PCR was performed in duplicate using TaqManTM Fast Advanced Master Mix (Cat # 44-445-57) for mRNA using a Mx3000p Real-Time PCR System (Stratagene, Santa Clara, CA). The primers for the QPCR were purchased from Thermo Fisher Scientific/TaqMan. Results for mRNA expression was normalized to internal control *Tuba1a*, and relative mRNA expression was determined using the ΔCt method.

Cell Culture: Human pulmonary artery smooth muscle cell (PASMCs; Purchased from Lonza, USA) were maintained at 37°C under 5% CO_2 in smooth muscle basal media (Lonza, #CC-3181) supplemented with growth factors (SMGM-2 smooth muscle singlequots kit, Lonza, #CC-4149). Once cells reached approximately 70% confluence, they were sub-cultured using 0.05% trypsin-EDTA (GIBCO, Cat # 25300-054, Thermo Fischer Scientific, Grand Island, NY) into 6-well plates at about $3x10^5$ cells/well.

Statistical analysis: Statistical analysis was performed using GraphPad Prism 5 software. Values are presented as mean ± standard error (SE). Statistical comparisons of samples were performed with two-way ANOVA followed by Sidak's post hoc test for multiple comparisons and Student's t test for comparing two groups. Difference with $P<0.05$ between the groups was considered significant.

JPET Fast Forward. Published on March 23, 2021 as DOI: 10.1124/jpet.120.000166
This article has not been copyedited and formatted. The final version may differ from this version.

Results

G6PD inhibition decreased chronic Hx- and Hx+SU-induced PH in mice: PH was induced by exposing C57BL/6J mice to Hx and Hx+SU (Figure 1A). C57BL/6J mice exposed to Hx and Hx+SU had higher RVSP and RVEDP than Nx mice (Figure 1B). In Nx+SU group as compared with Nx group, RVSP (Nx+SU: 24.6 ± 0.9 *vs* Nx: 23.2 ± 1.3; mmHg) and RVEDP (Nx+SU: 4.0 ± 0.4 *vs* Nx: 3.8 ± 0.4; mmHg) was not different. In Hx+SU group, RVSP and RVEDP were higher than those of Hx group (Figure 1B).

To determine whether G6PD inhibition reduces PH, we first established the maximum tolerated dose (MTD) of G6PD inhibitor (PDD4091). The MTD in Hx mice was 15 $mg.kg^{-1}.day^{-1}$ beyond which PDD4091 depressed LV function. More importantly, G6PD inhibitor, PDD4091, treatment to Hx mice decreased the elevated RVSP and RVEDP in a dose-dependent manner (Figure 1B and 1C top panel). PDD4091 had a reasonably wide therapeutic window (0.01 to 15 $mg.kg^{-1}.day^{-1}$) with an EC_{50} of 0.26±0.10 and 0.58±0.36 $mg.kg^{-1}.day^{-1}$ reduced both RVSP and RVEDP. Moreover, PDD4091 (1.5 $mg.kg^{-1}.day^{-1}$) treatment to both Hx and Hx+SU mice efficaciously reduced the elevated RVSP and RVEDP (Figure 1B and C bottom panel). Fulton's index was increased in Hx and Hx+SU groups as compared with Nx and Nx+SU groups. G6PD inhibitor reduced elevated Fulton's index in Hx and Hx+SU groups (Table 1). In addition, PDD4091 (1.5 $mg.kg^{-1}.day^{-1}$) treatment to mice (n=6) with pre-existing Hx+SU-induced PH reduced RVSP (from Hx+SU: 74±5.3 to Hx+SU+PDD4091: 41±3.3 mmHg; $P<0.05$), RVEDP (from Hx+SU: 13±3 to Hx+SU+PDD4091: 7±1mmHg; $P<0.05$), and Fluton's index (from Hx+SU: 0.4±0.01 to Hx+SU+PDD4091: 0.3±0.01; $P<0.05$). PDD4091 (1.5 $mg.kg^{-1}.day^{-1}$) reduced G6PD activity by 20%.

RV dp/dt had tendency to increase in Hx group compare to Nx, and significantly increased in Hx+SU compare to Nx. PDD4091 treatment (1.5 $mg.kg^{-1}.day^{-1}$; Table 1)

JPET Fast Forward. Published on March 23, 2021 as DOI: 10.1124/jpet.120.000166
This article has not been copyedited and formatted. The final version may differ from this version.

normalized RV dp/dt in Hx+SU group. LV hemodynamic and function parameters are shown in Table 2. There were no significant differences in mAP, LVSP, LVEDP and dp/dt in Hx and Hx+SU groups.

Next, we determined the effect of PPD4091 on hematocrit and organ (such as; liver, pancreas, and kidney) function. As expected, mice exposed to Hx had higher hematocrit than Nx (Table 2). Treating Hx mice with PDD4091 (1.5 $mg.kg^{-1}.day^{-1}$) for 3 weeks reduced the elevated hematocrit in Hx mice (Table 2). The blood chemistry analysis revealed that PDD4091 treatment normalized electrolyte levels and did not alter organ function in Hx mice (Table 3).

G6PD inhibition relaxed pre-contracted PA, decreased PASMC growth, and reduced PA remodeling in Hx+SU mice: PA remodeling is the hallmark of severe PH. Hyperplasic and apoptosis-resistant PA endothelial cells and PASMCs contribute to hypertensive remodeling (Morrell et al., 2009). Previously, we and others proposed that SMCs switch from a differentiated to a dedifferentiated phenotype in PA of hypertensive patients and animals and contribute to PA remodeling (Zhou et al., 2009; Chettimada et al., 2015; Sahoo et al., 2016). Dedifferentiated SMCs are hyper-proliferative, migratory, and secretory (Frismantiene et al., 2018). Previous studies show that the Hx+SU mouse model of PH has more severe PA remodeling than Hx mice (Vitali et al., 2014). Therefore, we determined whether G6PD inhibition relaxes PA in *ex vivo* studies, stunts the growth of PASMCs exposed to Hx and SU in cell culture, and reduces remodeling of PA in Hx+SU mice. Our results demonstrated PDD4091 dose-dependently relaxed PA pre-contracted with KCl (Figure 2A). Application of PDD4091 (1 μmol/L, an EC_{50} dose (Hamilton et al., 2012)) for 48 hours to PASMCs cultured in normoxia decreased cell numbers (Figure 2B) and in addition attenuated the cell growth evoked by Hx and Hx+SU (Figure 2C).

JPET Fast Forward. Published on March 23, 2021 as DOI: 10.1124/jpet.120.000166
This article has not been copyedited and formatted. The final version may differ from this version.

Treatment of Hx+SU mice with PDD4091 (1.5 $mg.kg^{-1}.day^{-1}$) for 3 weeks abrogated the occlusive pulmonary vascular remodeling (Figure 2D).

Gene expression is altered in lungs of Hx and Hx+SU mice: To discover the genetic and/or epigenetic determinants of PASMC growth in the PA wall and remodeling of PA in Hx and Hx+SU, we performed RNA-seq analysis in lungs of mice exposed to Nx, Hx, and Hx+SU. Several thousand genes (total 33,141) were up (15,412) or down (17,729) regulated in lungs of mice exposed to Hx and Hx+SU as compared with Nx. The results revealed that out of 159 and 97 genes upregulated (≥1.5log2_fold; *P*-value<0.05) in lungs of Hx vs Nx and Hx+SU vs Nx mice, respectively, only 3 genes were commonly upregulated in both groups (Figure 3A). Whereas out of 1511 and 1523 genes that were downregulated (≥1.5log2_fold; *P*-value<0.05) in lungs of Hx vs Nx and Hx+SU vs Nx mice, respectively, 1085 genes were commonly downregulated in both groups (Figure 3A). Transcription factor binding site enrichment analysis using oPOSSUM (Kwon et al., 2012) disclosed TCFCP2l1, KLF4, and E2F1 as the most enriched TFBS in genes upregulated in the Hx group and HIF1A::ARNT, KLF4, and SP1 as the most enriched TFBS in genes upregulated in the Hx+SU group (Figure 3B top panels). HOXA5, PDX1, and PRRX2 were the most enriched TFBS in genes downregulated in the Hx and Hx+SU groups (Figure 3B bottom panels). Suppressor of fused (*Sufu*) homolog and Cytochrome P450 1A1 (*Cyp1a1*) genes, respectively, upregulated >100- and >15-fold in lungs of mice exposed to Hx+SU, but not to Hx, while all genes downregulated >20-fold were common in lungs of mice exposed to Hx+SU and Hx (Figure 3C).

G6PD inhibition decreased expression of *Cyp1a1* and *Sufu* genes in lungs of mice and in human PASMCs exposed to Hx+SU: Next, we determined whether inhibition of G6PD activity decreases expression of *Cyp1a1* and *Sufu*, which are increased in lungs of hypertensive mice (Figure 3C), and in lungs of Hx and Hx+SU mice and in human

JPET Fast Forward. Published on March 23, 2021 as DOI: 10.1124/jpet.120.000166
This article has not been copyedited and formatted. The final version may differ from this version.

PASMCs exposed to Hx+SU. Treatment of PDD4091 (1.5 $mg.kg^{-1}.day^{-1}$) for 3 weeks to mice and application of PDD4091 (1 μM) to human PASMCs for 48 hr rescinded the Hx+SU-induced *Cyp1a1* and *Sufu* expression in lungs (Figure 4A, B) and in human PASMCs (Figure 4C).

Methylation of DNA is decreased in lungs of Hx and Hx+SU mice: Epigenetic modifications are incriminated in the pathogenesis of PH (Cheng et al., 2019). Recently, we reported that downregulation of ten-eleven translocation 2 (*Tet2*) DNA demethylase in lungs of Hx Sv129J mice lacking *Cyp2c44* gene contributes to the genesis of PH, and also demonstrated that inhibition of G6PD was ineffective in reducing PH in hypoxic *Tet2*$^{-/-}$ mice (Joshi et al., 2020). Therefore, we assumed that downregulation of *Tet2* by Hx may augment DNA methylation in C57BL/6J mice and mediate maladaptive gene expression. Unexpectedly, we found that expression of *Tet1*, but not of *Tet2* or *Tet3*, was reduced in lungs of C57BL/6J mice exposed to Hx (Figure 5A and Table 4). In addition, expression of *Dnmt3b*, but not of *Dnmt3a* or *Dnmt1a*, was decreased (Figure 5A and Table 4). Concomitantly, we found that 45,321 CpG regions were differentially methylated out of which 46.53% regions were hypermethylated and 53.47% were hypomethylated in lungs of mice exposed to Hx as compared with Nx (Figure 5B). While 46,286 CpG regions were differentially methylated out of which 46.15% regions were hypermethylated and 53.85% were hypomethylated in lungs of mice exposed to Hx+SU as compared with Nx (Figure 5C). Therefore, there were 0.38% more hypomethylated and less hypermethylated CpG regions in lungs of Hx+SU vs Nx than Hx vs Nx C57BL/6J mice. Furthermore, two genes, *Cyp1a1* and *Kcng3*, out of 12 up-regulated genes (Figure 3C), were hypomethylated in lungs of both Hx vs Nx and Hx+SU vs Nx C57BL/6J mice (Figure 5D). It is noteworthy that CpG regions 2890 bp from the transcription start site of *Cyp1a1* gene were

JPET Fast Forward. Published on March 23, 2021 as DOI: 10.1124/jpet.120.000166
This article has not been copyedited and formatted. The final version may differ from this version.

hypomethylated in both Hx vs Nx and Hx+SU vs Nx groups (Figure 5D), and G6PD inhibition hypermethylated *Cyp1a1* and *Kcng3* genes (Table 5).

JPET Fast Forward. Published on March 23, 2021 as DOI: 10.1124/jpet.120.000166
This article has not been copyedited and formatted. The final version may differ from this version.

Discussion

Pharmacologic inhibition of G6PD activity, with a selective and potent inhibitor synthesized so far/to-date, relaxed pre-contracted PA, decreased growth of PASMCs evoked by Hx and SU, reduced expression of *Cyp1a1* and *Sufu* and rescinded occlusion of PA in lungs of mice exposed to Hx+SU. Furthermore, the results of this study provided evidence that downregulation of the epigenetic modifiers *Tet1* and *Dnmt3b* and hypomethylation of DNA altered gene expression in lungs of Hx- and Hx+SU mice. Since a selective inhibitor of G6PD activity decreased occlusive remodeling of PA and alleviated RVSP/heart dysfunction evoked by Hx and Hx+SU in mice, without causing organ toxicity in Hx mice, we propose that G6PD might be a safe pharmacotherapeutic target to reduce pre-capillary PH.

Hx and Hx+SU mouse models are routinely used to study the pathology of PH (Stenmark et al., 2009). We observed in this study that mice exposed to Hx for 6 weeks and to Hx+SU for 3 weeks developed PH, which was more severe in Hx+SU than Hx group. In chronically Hx (3 weeks) mice, vasoconstriction and muscularization of small arteries, but not obliterative remodeling of PA, contribute to increased pulmonary arterial pressure and RV pressure overload (Stenmark et al., 2009). The more severe PH in Hx+SU mice is attributed to the formation of angio-obliterative lesions in addition to vasoconstriction and muscularization (Vitali et al., 2014). Along with vascular pathology, RV pressure and contractility increased in Hx and Hx+SU group. Systemic blood pressure (mAP) and LV hemodynamic (LVSP, LVEDP and dp/dt) was not significantly different in Hx and Hx+SU group compared to their control groups. Thus, our results indicate that inhibition of G6PD activity reduces both remodeling of PA and elevated RV pressure overload and hypertrophy in two different mice models of PH.

The above observations raise the question of whether the underlying genetic/epigenetic determinants of PH in mice exposed to Hx and Hx+SU are same or different? To seek answers, we performed RNA-seq analysis in lungs which revealed that

JPET Fast Forward. Published on March 23, 2021 as DOI: 10.1124/jpet.120.000166
This article has not been copyedited and formatted. The final version may differ from this version.

>1000 downregulated genes and only 3 upregulated genes, driven by different transcription factors, were common between the two models. Most strikingly, expression of *Sufu* and *Cyp1a1* genes increased >15-fold in lungs of mice exposed to Hx+SU but not to Hx. Furthermore, exposure to SU increased expression of both *SUFU* and *CYP1A1* genes in Hx but not in Nx human PASMCs. While these results are consistent with a recent study that indicates HIF::ART-driven *Cyp1a1* gene is upregulated in lungs of rats exposed to SU/Hx/Nx and in human PASMCs by SU (Dean et al., 2018), an increase of *Sufu* in lungs of PH mice and human PASMCs has not been reported. CYP1A1 is an estrogen-metabolizing enzyme that produces mitogenic metabolites of estrogen in human PASMCs (Dean et al., 2018) and SUFU is a negative regulator of hedgehog signaling, which controls cell proliferation during development in invertebrates and vertebrates (Briscoe and Therond, 2013; Liu, 2019). Increased CYP1A1 contributes to the pathogenesis of PH in SU/Hx/Nx rats (Dean et al., 2018). Our results suggest that increased CYP1A1 and SUFU signaling may have a potential role in the genesis of occlusive lesion formation in Hx+SU mice. Since transcription of *CYP1A1* was abolished and that of *SUFU* was partially decreased in mice lungs and in human PASMCs by G6PD inhibition, transcription of *CYP1A1* and *SUFU* genes in lungs and PASMCs exposed to Hx+SU is potentially controlled by G6PD. Therefore, we propose inhibition of G6PD activity could be useful in reversing the elevated expression of the pathogenic *CYP1A1* and *SUFU* genes in PH.

We and others have recently proposed that DNA methylation and other epigenetic modifications potentially promote maladaptive gene expression, a determinant of inflammatory and hyperproliferative cell phenotype, in remodeled PA (Hu et al., 2019; Joshi et al., 2020; Potus et al., 2020). Furthermore, we recently showed that expression of *Tet2*, a DNA demethylase considered as a master regulator of differentiated fate of SMC

JPET Fast Forward. Published on March 23, 2021 as DOI: 10.1124/jpet.120.000166
This article has not been copyedited and formatted. The final version may differ from this version.

phenotype (Liu et al., 2013), was downregulated in lungs of Sv129J mice with a *Cyp2c44* gene knockout (Joshi et al., 2020). Therefore, we assumed that a loss of TET2 modifies DNA methylation and initiates maladaptive gene expression in lungs of mice exposed to Hx and Hx+SU. Unexpectedly, expression of *Tet1*, but not of *Tet2,* and *Dnmt3b* was downregulated in lungs of C57BL/6J mice exposed to Hx and Hx+SU. We propose genetic variations and differences in gene regulation observed between Sv129J and C57BL/6J mice (Hashimoto et al., 2020) may be a cause of *Tet1* and *Dnmt3b* downregulation, but not of other isoforms of DNA demethylases and methyltransferases, in response to stress observed in C57BL/6J mice. TET proteins are involved in the regulation of hematopoietic stem cell homeostasis, and hematological malignancies and diseases (Nakajima and Kunimoto, 2014). Although loss of single TET protein is not sufficient to promote malignancies (An et al., 2015), TET1 and TET2 have been shown to, respectively, repress and promote osteogenesis and adipogenesis (Cakouros et al., 2019). Furthermore, inhibition of TET1 blocks expression of large-conductance Ca^{2+}-activated K^+ channel β1 subunit in uterine arteries of pregnant rats (Hu et al., 2017). Expression of this channel is a marker of differentiated SMCs. Therefore, we propose that downregulation of *Tet1* could imply that: 1) SMCs are dedifferentiated and 2) decreased Ca^{2+}-activated K^+ channels contribute to constrict PAs and increase pressure in lungs of Hx and Hx+SU mice.

While inhibition of G6PD evoked hypomethylation and increased transcription of the many genes, expression of *Cyp1a1* gene that promotes PASMC proliferation (Dean et al., 2018) was repressed through hypermethylation of the DNA in lungs of Hx and Hx+SU mice. Therefore, these results suggest that DNA methylation modulated by G6PD is functionally important in gene regulation and substantiate our previous finding that G6PD is a regulator of DNA methyltransferases and demethylase, which plays a crucial role in remodeling of PA (Joshi et al., 2020). In contrast, transcription of *Sufu* in mouse lungs

JPET Fast Forward. Published on March 23, 2021 as DOI: 10.1124/jpet.120.000166
This article has not been copyedited and formatted. The final version may differ from this version.

evoked by Hx+SU was not regulated by the methylation of DNA. These results suggest G6PD inhibition activated other mechanisms of gene expression in addition to differential methylation of the DNA, and these mechanisms worked synergistically to regulate gene expression in lungs of Hx and Hx+SU mice.

In addition to arresting maladaptive gene expression in vascular cells of the PA wall and reducing cell growth in occlusive pulmonary arterial disease, PDD4091 – a novel and selective inhibitor of G6PD activity (Hamilton et al., 2012) – dose-dependently relaxed pre-contracted PAs. We have previously shown that inhibition of G6PD activity with non-specific inhibitors, such as 17-ketosteroids (dehydroepiandrosterone (DHEA) and epiandrosterone – a DHEA metabolite), and siRNA-mediated knockdown of *G6pd*, elicits relaxation of pre-contracted pulmonary artery (Gupte et al., 2002) and reduces RV pressures in hypertensive rats (Chettimada et al., 2012; Chettimada et al., 2015). Therefore, these studies and our current findings collectively suggest that G6PD inhibition reduces the elevated RV pressures and PH in Hx- and Hx+SU mice by dilating PAs and reducing PA remodeling.

In conclusion, our results collectively demonstrate that G6PD activity is an important contributor to differential DNA methylation, maladaptive gene expression, and remodeling of PA in Hx and Hx+SU mice. The inhibition of G6PD activity by pharmacologic manipulations abrogated pulmonary vascular remodeling and improved the hemodynamics in mouse models of PH. Therefore, G6PD inhibitor, N-[(3β,5α)-17-Oxoandrostan-3-yl]sulfamide, might be employed in the future as a pharmacotherapeutic agent to treat different forms of PH.

JPET Fast Forward. Published on March 23, 2021 as DOI: 10.1124/jpet.120.000166
This article has not been copyedited and formatted. The final version may differ from this version.

Acknowledgments: None.

JPET Fast Forward. Published on March 23, 2021 as DOI: 10.1124/jpet.120.000166
This article has not been copyedited and formatted. The final version may differ from this version.

Authors Contributions:

Participated in research design: Gupte, McMurtry, and Kitagawa

Conducted experiments: Kitagawa and Jacob

Contributed new reagents or analytic tools: Jordan and Waddell

Performed data analysis: Kitagawa, Jacob, and Gupte

Wrote or contributed to the writing of the manuscript: Gupte, Kitagawa, Jacob, McMurtry

References

An J, Gonzalez-Avalos E, Chawla A, Jeong M, Lopez-Moyado IF, Li W, Goodell MA, Chavez L, Ko M and Rao A (2015) Acute loss of TET function results in aggressive myeloid cancer in mice. *Nat Commun* **6**:10071.

Boucherat O, Vitry G, Trinh I, Paulin R, Provencher S and Bonnet S (2017) The cancer theory of pulmonary arterial hypertension. *Pulm Circ* **7**:285-299.

Briscoe J and Therond PP (2013) The mechanisms of Hedgehog signalling and its roles in development and disease. *Nat Rev Mol Cell Biol* **14**:416-429.

Cakouros D, Hemming S, Gronthos K, Liu R, Zannettino A, Shi S and Gronthos S (2019) Specific functions of TET1 and TET2 in regulating mesenchymal cell lineage determination. *Epigenetics Chromatin* **12**:3.

Cheng X, Wang Y and Du L (2019) Epigenetic Modulation in the Initiation and Progression of Pulmonary Hypertension. *Hypertension* **74**:733-739.

Chettimada S, Gupte R, Rawat D, Gebb SA, McMurtry IF and Gupte SA (2015) Hypoxia-induced glucose-6-phosphate dehydrogenase overexpression and -activation in pulmonary artery smooth muscle cells: implication in pulmonary hypertension. *Am J Physiol Lung Cell Mol Physiol* **308**:L287-300.

Chettimada S, Rawat DK, Dey N, Kobelja R, Simms Z, Wolin MS, Lincoln TM and Gupte SA (2012) Glc-6-PD and PKG contribute to hypoxia-induced decrease in smooth muscle cell contractile phenotype proteins in pulmonary artery. *Am J Physiol Lung Cell Mol Physiol* **303**:L64-74.

D'Alessandro A, El Kasmi KC, Plecita-Hlavata L, Jezek P, Li M, Zhang H, Gupte SA and Stenmark KR (2018) Hallmarks of Pulmonary Hypertension: Mesenchymal and Inflammatory Cell Metabolic Reprogramming. *Antioxid Redox Signal* **28**:230-250.

Dean A, Gregorc T, Docherty CK, Harvey KY, Nilsen M, Morrell NW and MacLean MR (2018) Role of the Aryl Hydrocarbon Receptor in Sugen 5416-induced Experimental Pulmonary Hypertension. *Am J Respir Cell Mol Biol* **58**:320-330.

Farber HW and Loscalzo J (2004) Pulmonary arterial hypertension. *N Engl J Med* **351**:1655-1665.

Frismantiene A, Philippova M, Erne P and Resink TJ (2018) Smooth muscle cell-driven vascular diseases and molecular mechanisms of VSMC plasticity. *Cell Signal* **52**:48-64.

Gupte SA, Li KX, Okada T, Sato K and Oka M (2002) Inhibitors of pentose phosphate pathway cause vasodilation: involvement of voltage-gated potassium channels. *J Pharmacol Exp Ther* **301**:299-305.

Hamilton NM, Dawson M, Fairweather EE, Hamilton NS, Hitchin JR, James DI, Jones SD, Jordan AM, Lyons AJ, Small HF, Thomson GJ, Waddell ID and Ogilvie DJ (2012) Novel steroid inhibitors of glucose 6-phosphate dehydrogenase. *J Med Chem* **55**:4431-4445.

Hashimoto R, Lanier GM, Dhagia V, Joshi SR, Jordan A, Waddell I, Tuder R, Stenmark KR, Wolin MS, McMurtry IF and Gupte SA (2020) Pluripotent hematopoietic stem cells augment alpha-adrenergic receptor-mediated contraction of pulmonary artery and contribute to the pathogenesis of pulmonary hypertension. *Am J Physiol Lung Cell Mol Physiol* **318**:L386-L401.

Hu CJ, Zhang H, Laux A, Pullamsetti SS and Stenmark KR (2019) Mechanisms contributing to persistently activated cell phenotypes in pulmonary hypertension. *J Physiol* **597**:1103-1119.

Hu XQ, Dasgupta C, Chen M, Xiao D, Huang X, Han L, Yang S, Xu Z and Zhang L (2017) Pregnancy Reprograms Large-Conductance Ca(2+)-Activated K(+) Channel in Uterine Arteries: Roles of Ten-Eleven Translocation Methylcytosine Dioxygenase 1-Mediated Active Demethylation. *Hypertension* **69**:1181-1191.

Joshi SR, Kitagawa A, Jacob C, Hashimoto R, Dhagia V, Ramesh A, Zheng C, Zhang H, Jordan A, Waddell I, Leopold J, Hu CJ, McMurtry IF, D'Alessandro A, Stenmark KR and Gupte SA (2020) Hypoxic activation of glucose-6-phosphate dehydrogenase controls the expression of genes involved in the pathogenesis of pulmonary hypertension through the regulation of DNA methylation. *Am J Physiol Lung Cell Mol Physiol* **318**:L773-L786.

Kwon AT, Arenillas DJ, Worsley Hunt R and Wasserman WW (2012) oPOSSUM-3: advanced

analysis of regulatory motif over-representation across genes or ChIP-Seq datasets. *G3* **2**:987-1002.

Lajoie AC, Lauziere G, Lega JC, Lacasse Y, Martin S, Simard S, Bonnet S and Provencher S (2016) Combination therapy versus monotherapy for pulmonary arterial hypertension: a meta-analysis. *Lancet Respir Med* **4**:291-305.

Liu A (2019) Proteostasis in the Hedgehog signaling pathway. *Semin Cell Dev Biol* **93**:153-163.

Liu R, Jin Y, Tang WH, Qin L, Zhang X, Tellides G, Hwa J, Yu J and Martin KA (2013) Ten-eleven translocation-2 (TET2) is a master regulator of smooth muscle cell plasticity. *Circulation* **128**:2047-2057.

Morrell NW, Adnot S, Archer SL, Dupuis J, Jones PL, MacLean MR, McMurtry IF, Stenmark KR, Thistlethwaite PA, Weissmann N, Yuan JX and Weir EK (2009) Cellular and molecular basis of pulmonary arterial hypertension. *J Am Coll Cardiol* **54**:S20-31.

Nakajima H and Kunimoto H (2014) TET2 as an epigenetic master regulator for normal and malignant hematopoiesis. *Cancer Sci* **105**:1093-1099.

Potus F, Pauciulo MW, Cook EK, Zhu N, Hsieh A, Welch CL, Shen Y, Tian L, Lima P, Mewburn J, D'Arsigny CL, Lutz KA, Coleman AW, Damico R, Snetsinger B, Martin AY, Hassoun PM, Nichols WC, Chung WK, Rauh MJ and Archer SL (2020) Novel Mutations and Decreased Expression of the Epigenetic Regulator TET2 in Pulmonary Arterial Hypertension. *Circulation*.

Runo JR and Loyd JE (2003) Primary pulmonary hypertension. *Lancet* **361**:1533-1544.

Sahoo S, Meijles DN, Al Ghouleh I, Tandon M, Cifuentes-Pagano E, Sembrat J, Rojas M, Goncharova E and Pagano PJ (2016) MEF2C-MYOCD and Leiomodin1 Suppression by miRNA-214 Promotes Smooth Muscle Cell Phenotype Switching in Pulmonary Arterial Hypertension. *PLoS One* **11**:e0153780.

Stenmark KR, Meyrick B, Galie N, Mooi WJ and McMurtry IF (2009) Animal models of pulmonary arterial hypertension: the hope for etiological discovery and pharmacological cure. *Am J Physiol Lung Cell Mol Physiol* **297**:L1013-1032.

Vitali SH, Hansmann G, Rose C, Fernandez-Gonzalez A, Scheid A, Mitsialis SA and

Kourembanas S (2014) The Sugen 5416/hypoxia mouse model of pulmonary hypertension revisited: long-term follow-up. *Pulm Circ* **4**:619-629.

Warburg O, Wind F and Negelein E (1927) The Metabolism of Tumors in the Body. *J Gen Physiol* **8**:519-530.

Zhou W, Negash S, Liu J and Raj JU (2009) Modulation of pulmonary vascular smooth muscle cell phenotype in hypoxia: role of cGMP-dependent protein kinase and myocardin. *Am J Physiol Lung Cell Mol Physiol* **296**:L780-789.

Footnotes:

Funding: This study was supported by: National Heart, Blood, and Lung Institute (Grant Number: RO1HL132574 to SAG), American Heart Association Grant-in-Aid (Grant Number: 17GRNT33670454 to SAG), and Cancer Research UK (Grant numbers C480/A1141 and C5759/A17098 to AJ and IW). Some parts of the results were presented at American Heart Association Scientific Session 2019 at Philadelphia, PA, USA.

Conflict of Interest: None declared.

JPET Fast Forward. Published on March 23, 2021 as DOI: 10.1124/jpet.120.000166
This article has not been copyedited and formatted. The final version may differ from this version.

Figure Legends:

Figure 1: Daily injection of a novel G6PD inhibitor, PDD4091, decreased pulmonary artery remodeling, and right ventricle pressure and hypertrophy, in mice elicited by hypoxia and hypoxia+Sugen5416. A) A schematic showing various treatment protocols in C57BL/6J mice in normoxia and hypoxia, and mice treated with Sugen5416 (20 $mg.kg^{-1}$) once a week. B and C) Right ventricle systolic (RVSP) and diastolic (RVDP) pressure was reduced dose-dependently by PDD4091 treatment for 3 weeks to hypoxic mice. PDD4091 (1.5 $mg.kg^{-1}.day^{-1}$) for 3 weeks reduced RVSP and RVDP in mice exposed to hypoxia and hypoxia+Sugen5416. N=11, normoxia; N=6, normoxia+4091; N=9, hypoxia; N=6, hypoxia+4091 (0.10 $mg.kg^{-1}.day^{-1}$); N=11, hypoxia+4091 (1.5 $mg.kg^{-1}.day^{-1}$); N=6, hypoxia+4091 (15 $mg.kg^{-1}.day^{-1}$); N=5, hypoxia+Sugen5416 (20 $mg.kg^{-1}$); and N=5, hypoxia+Sugen5416 (20 $mg.kg^{-1}$)+ 4091 (1.5 $mg.kg^{-1}.day^{-1}$). Each group included male and female mice (2:1 ratio). Statistical analysis was performed using Two-way ANOVA and Sidak's test for multiple comparisons.

Figure 2: G6PD inhibitor, PDD4091, relaxed pre-contracted PA, decreased PASMC growth, and rescinded occlusive lesion in PA. A) Application of PDD4091 dose-dependently relaxed the pulmonary arterial rings pre-contracted with KCl (30 mM), N=6 in each dose. B) Application of PDD4091 (1 μmol/L) to human pulmonary artery smooth muscle cells for 48 hours decreased growth of cells cultured in 21% O_2, N=6. C) Hypoxia (3% O_2; N=6) and Sugen (1 μmol/L; N=6), as compared with normoxia-control (21% O_2; N=6), increased human pulmonary artery smooth muscle cell numbers, and application of PDD4091 (1 μmol/L; N=6) to cells for 48 hr reduced their growth. D) Immunofluorescent micrograph shows occluded pulmonary artery in lungs of mice exposed to hypoxia+Sugen5416 (SU), and occluded pulmonary arteries were not present in

JPET Fast Forward. Published on March 23, 2021 as DOI: 10.1124/jpet.120.000166
This article has not been copyedited and formatted. The final version may differ from this version.

lungs of hypoxia+Sugen5416 (SU) mice treated with PDD4091 for 3 weeks. N=4 in normoxia; hypoxia+Sugen5416 (SU) and hypoxia+Sugen5416 (SU)+4091 groups. *P<0.05 vs $3x10^{-9}$ M in panel A. *P<0.05 vs control or normoxia (Nx), and #P<0.05 vs hypoxia in panel B and C. Statistical analysis was performed by One-way ANOVA in panel A and C, and by Student's *t*-test in panel B.

Figure 3: Gene expression in lungs of mice exposed to hypoxia and hypoxia+Sugen5416. A) Venn diagram of whole-genome RNA-seq analysis demonstrate 3 genes are common in significantly up regulated cohort and 1085 genes are common in significantly down regulated cohort in lungs of mice exposed to hypoxia (Hx) and hypoxia+Sugen (Hx+SU) compared to normoxia-control (Nx). B) Transcription factor binding site enrichment analysis using oPPOSUM revealed TCFCP2L1 and KLF4 in Hx vs Nx and HIF1A::ARNT and KLF4 in Hx+SU vs Nx are the most enriched TFBS in genes up regulated category, and REST and HOXA5 in Hx vs Nx and HOXA5 and PDX1 in Hx+SU vs Nx are the enriched TFBS in genes down regulated category in mice lungs. C) RNA-seq results demonstrate *Sufu* and *Cyp1a1* genes are most up regulated in lungs of mice exposed to Hx+SU vs Nx but not to Hx vs Nx, and *Tubg2* and *Sv2b* genes are most down regulated in lungs of mice exposed to Hx+SU vs Nx and to Hx vs Nx. RNA-seq was performed on three lungs in each group. Male=2 and female=1. For statistical analysis the Benjamini-Hochberg method was applied for multiple test correction (FDR<0.05).

Figure 4. Expression of *Cyp1a1* and *Sufu* genes is decreased by G6PD inhibitor, PDD4091. A, B) Real-time PCR results confirmed RNA-seq results that *Cyp1a1* and *Sufu* are increased in lungs of mice exposed to Hx+SU but not to Hx, and PDD4091 treatment decreased *Cyp1a1* and *Sufu*. N=5 (male=3 and female=2) were used for qPCR analysis in

JPET Fast Forward. Published on March 23, 2021 as DOI: 10.1124/jpet.120.000166
This article has not been copyedited and formatted. The final version may differ from this version.

each group. C) Expression of *CYP1A1* and *SUFU* increased in human pulmonary artery smooth muscle cells cultured in hypoxia (3 % O_2), but not in normoxia (21% O_2), by Sugen5416 (SU: 1 μmol/L). Application of PDD4091 (1 μmol/L) to cells for 48 hr rescinded their elevated expression of *CYP1A1* and *SUFU*. N=6 in each experimental condition. Statistical analysis was performed using Two-way ANOVA and Sidak's test for multiple comparisons.

Figure 5. DNA methylation in lungs of mice exposed to hypoxia and hypoxia+Sugen5416. A) RNA-seq results disclosed that expression of ten-eleven translocation 1 demethylase (*Tet1*) and DNA methyltransferase 3b (*Dnmt3b*) genes are significantly decreased in lungs of mice exposed to hypoxia (Hx) and hypoxia+Sugen5416 (Hx+SU) as compared with normoxia (Nx). N=3 in each group. Methylation of the DNA in lungs of mice exposed to Nx, Hx and Hx+SU was determined by Reduced Representation Bisulfite Sequencing method. B, C) Pie graph demonstrate more CpG regions are hypomethylated in lungs Hx vs Nx and Hx+SU vs Nx mice. D) *Cyp1a1* and *Kcng3* genes are hypomethylated in lungs of Hx and Hx+SU mice. The statistical differences in differential methylation between conditional groups was performed using the Chi-squared test and applying a *q*-value (SLIM) threshold of 0.05 and a methylation difference threshold of 25 percent.

JPET Fast Forward. Published on March 23, 2021 as DOI: 10.1124/jpet.120.000166
This article has not been copyedited and formatted. The final version may differ from this version.

Table 1: RV contractility and hypertrophy in normoxia (Nx)-control vs. PH groups.

	Nx (n = 11)	Nx+4091 (n = 6)	Hx (n = 9)	Hx+4091 (n = 11)	Hx+SU (n = 7)	Hx+SU+4091 (n = 6)
RV dP/dt max (mmHg/s)	1664±391	1343±289	2567± 1745	1437 ± 390	2706 ± 703*	1647 ± 114¶
RV -dP/dt min (mmHg/s)	5266±1029	5890 ± 570	4945 ± 788	4753 ± 553	4648 ± 1099	4504 ± 1302
Fulton's index, RV/LV+S	0.225±0.035	0.249±0.040	0.385±0.080***	0.202±0.032§§§	0.388±0.030***	0.291±0.031¶¶¶

The statistical differences between groups was determined by two-way ANOVA followed by Sidak's post hoc test. RV: right ventricle; RV Ees: right ventricle end-systolic elastance; and Ea: arterial elastance. Comparison with Nx; *: $p < 0.05$; **: $p < 0.001$; ***: $p < 0.0001$; Comparison with Hx; §: $p < 0.05$; §§: $p < 0.01$; §§§: $p < 0.001$; and Comparison with SuHx; ¶: $p < 0.05$; ¶¶: $p < 0.001$; ¶¶¶: $p < 0.0001$.

JPET Fast Forward. Published on March 23, 2021 as DOI: 10.1124/jpet.120.000166
This article has not been copyedited and formatted. The final version may differ from this version.

Table 2: Systemic blood pressure, LV hemodynamic, and hematocrit changes in normoxia (Nx)-control and treatments groups.

	Nx (n = 11)	Nx + 4091 (n = 6)	Hx (n = 9)	Hx + 4091 (n = 11)	SuHx (n = 7)	SuHx + 4091 (n = 6)
BW (g)	23 ± 3	26 ± 5	24 ± 3	23 ± 3	25 ± 3	26 ± 2
HR (bpm)	455 ± 71	508 ± 71	455 ± 36	466 ± 34	519 ± 19	408 ± 52¶¶
mAP (mmHg)	87.7 ± 12.4	76.5 ± 4.0*	88.3 ± 6.7	85.4 ± 4.8	82.2 ± 15.3	85.0 ± 4.0
LV SP (mmHg)	104.0 ± 11.2	95.5 ± 3.9	104.8 ± 5.7	96.8 ± 3.9	101.8 ± 21.2	97.9 ± 4.6
LV EDP (mmHg)	11.2 ± 2.8	6.2 ± 3.2	15.2 ± 3.2	10.7 ± 1.9	16.5 ± 9.9	7.9 ± 2.3
dP/dt max (mmHg/s)	5841 ± 803	6385 ± 462	5559 ± 496	5567 ± 668	6021 ± 1114	5510 ± 1302
-dP/dt min (mmHg/s)	5266 ± 1029	5890 ± 570	4945 ± 788	4753 ± 553	4648 ± 1099	4504 ± 1302
Ht (%)	46 ± 3	44 ± 2	60 ± 3***	48 ± 6§§§	59 ± 3***	56 ± 4

The statistical differences between groups was determined by two-way ANOVA followed by Sidak's post hoc test. Body weight, BW; Heart rate, HR; Systemic mean arterial pressure, mAP; Left ventricle end systolic pressure, LVSP; Left ventricle end diastolic pressure, LVEDP; Cardiac index, CI; Hematocrit, Ht. Comparison with Nx; *: $p < 0.05$; **: $p < 0.001$; ***: $p < 0.0001$; Comparison with Hx; §: $p < 0.05$; §§: $p < 0.01$; §§§: $p < 0.001$; and Comparison with SuHx; ¶: $p < 0.05$; ¶¶: $p < 0.001$; ¶¶¶: $p < 0.0001$.

JPET Fast Forward. Published on March 23, 2021 as DOI: 10.1124/jpet.120.000166
This article has not been copyedited and formatted. The final version may differ from this version.

Table 3: Blood chemistry in mice.

Blood Parameters	Nx	Hx	Hx+4091
Blood urea nitrogen (mg/dl)	31.3±3.8	31.8±1.4	36.0±2.0
Creatinine (mg/dl)	0.23±0.03	0.20±0.0	0.23±0.03
Glucose (mg/dl)	115±33	127±18	145±19
Na^+ (mmol/L)	162±1	182±2*	168±3#
K^+ (mmol/L)	4.6±0.4	3.5±0.1*	4.8±0.4#
Cl^- (mmol/L)	125±1	118±1*	127±3#
Alkaline phosphatase (U/L)	49±4	68±8*	40±4#
Alanine aminotransferase (U/L)	9±2	6±1	5±2
Aspartate aminotransferase (U/L)	75±6	106±28	75±2
Total bilirubin (mg/dl)	0.1±0.0	0.1±0.0	0.1±0.0
Direct bilirubin (mg/dl)	0±0	0±0	0±0
Lactate dehydrogenase (U/L)	374±78	367±39	449±22
Creatine kinase (U/L)	254±57	268±68	136±21
Total protein (g/dl)	3.6±0.1	3.2±0.1*	3.7±0.1#
Albumin (g/dl)	2.1±0.1	1.1±0.1*	2.1±0.1#
Ca^{2+} (mg/dl)	7.6±0.2	6.6±0.1*	7.2±0.2#
PHOS (mg/dl)	9.2±1.7	8.3±0.9	9.4±1.2
Mg^+ (mg/dl)	2.2±0.1	2.2±0.1	2.3±0.3
Cholesterol (mg/dl)	44±8	52±3	66±7
Triglycerides (mg/dl)	46±13	82±15	64±9
Amylase (U/L)	406±64	300±13	387±34
Lipase (U/L)	87±20	45±6*	42±7*

The statistical differences between groups was determined by two-way ANOVA followed by Sidak's post hoc test. *P<0.05 vs Nx and #P<0.05 vs Hx

JPET Fast Forward. Published on March 23, 2021 as DOI: 10.1124/jpet.120.000166
This article has not been copyedited and formatted. The final version may differ from this version.

Table 4: Expression of *Dnmt* and *Tet* genes in mouse lungs.

Genes	Hx vs Nx		Hx+SU5149 vs Nx	
	Log2_fold	*P*-value	Log2_fold	*P*-value
Dmnt1	-0.775	0.1700	-1.377	0.0158
Dnmt3a	0.086	0.8400	0.969	0.0200
Dnmt3b	-3.056	0.0028	-3.101	0.0032
Tet1	-2.219	0.0195	-1.852	0.0472
Tet2	0.628	0.2479	0.440	0.4165
Tet3	0.212	0.4949	0.402	0.1886

For statistical analysis the Benjamini-Hochberg method was applied for multiple test correction (FDR<0.05).

JPET Fast Forward. Published on March 23, 2021 as DOI: 10.1124/jpet.120.000166
This article has not been copyedited and formatted. The final version may differ from this version.

Table 5: Methylation status of *Cyp1a1* and *Kcng3* gene in mouse lungs.

Condition	Gene Name	Strand	Distance from TSS	% Differential Methylation	q-value (SLIM)
Hx vs Nx	ENSMUST00000034865.4_Cyp1a1	+	2890	-36.1	1.42E-05
		+	3890	-25.1	0.00366025
		+	4390	-31.4	2.25E-13
Hx+SU vs Nx	ENSMUST00000034865.4_Cyp1a1	+	2890	-41.9	3.63E-07
Hx+4091 vs Hx	ENSMUST00000034865.4_Cyp1a1	+	2890	36.1	7.35E-06
		+	3890	86.4	5.33E-31
		+	4390	55.0	4.27E-26
Hx vs Nx	ENSMUST00000051482.1_Kcng3	-	36396	-26.7	0.00044669
Hx+SU vs Nx	ENSMUST00000051482.1_Kcng3	-	34396	-29.1	3.44E-14
Hx+4091 vs Hx	ENSMUST00000051482.1_Kcng3	-	36396	26.7	0.00245735
		-	34396	-51.7	5.03E-26

The statistical differences in differential methylation between conditional groups was performed using the Chi-squared test and applying a *q*-value (SLIM) threshold of 0.05 and a methylation difference threshold of 25 percent.

JPET Fast Forward. Published on March 23, 2021 as DOI: 10.1124/jpet.120.000166
This article has not been copyedited and formatted. The final version may differ from this version.

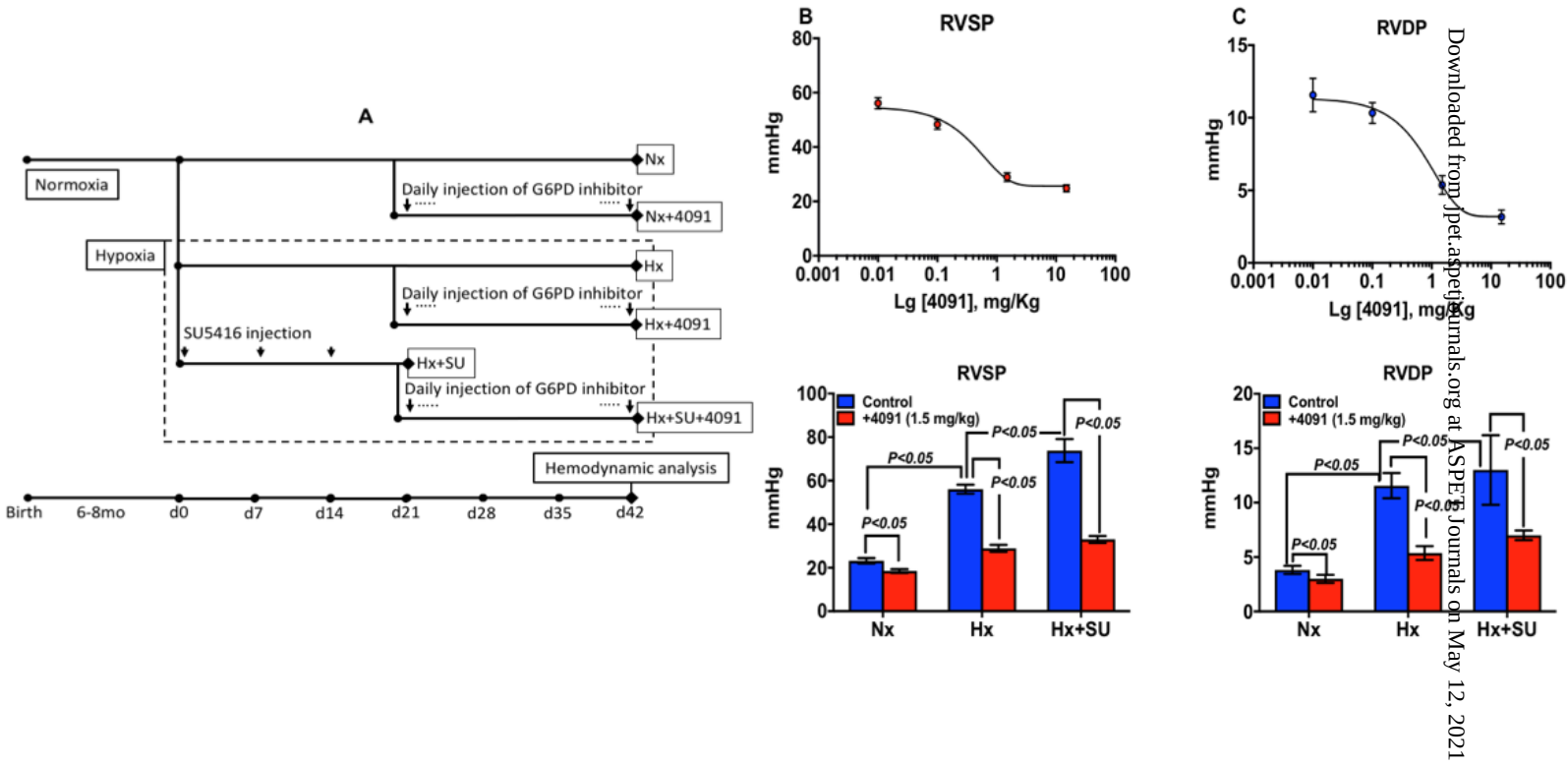

JPET Fast Forward. Published on March 23, 2021 as DOI: 10.1124/jpet.120.000166
This article has not been copyedited and formatted. The final version may differ from this version.

Fig 2

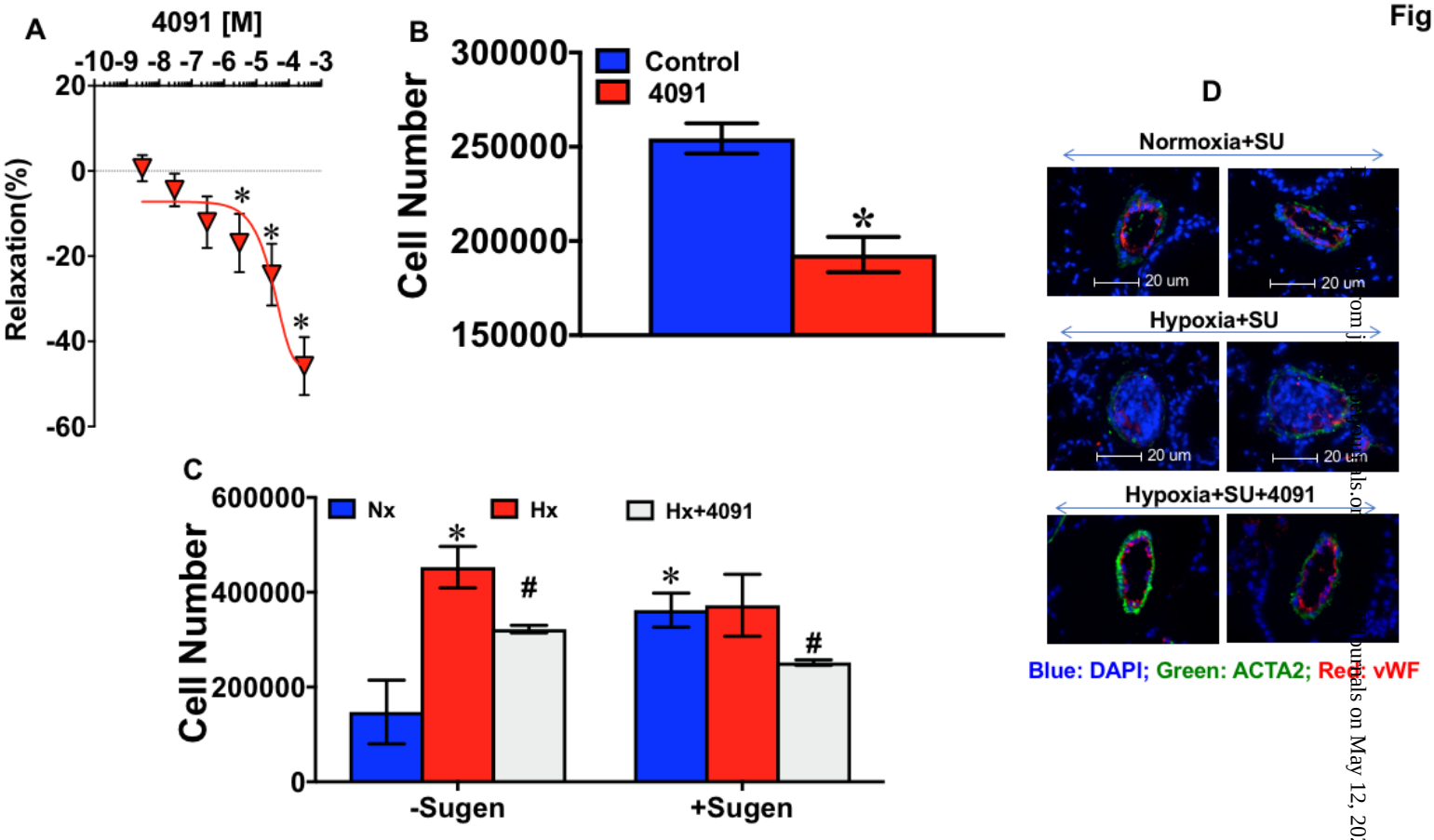

JPET Fast Forward. Published on March 23, 2021 as DOI: 10.1124/jpet.120.000166
This article has not been copyedited and formatted. The final version may differ from this version.

Fig 3

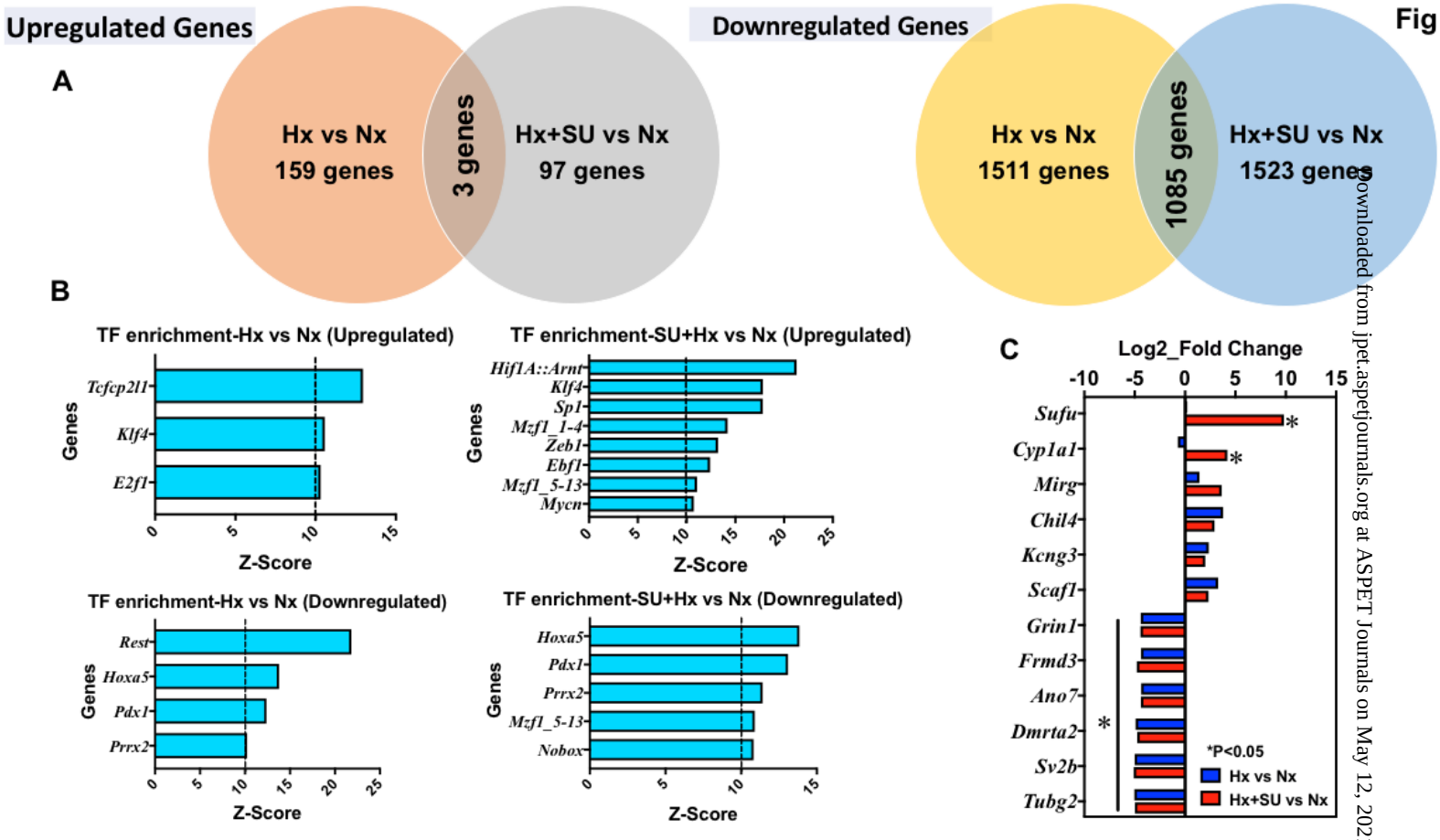

JPET Fast Forward. Published on March 23, 2021 as DOI: 10.1124/jpet.120.000166
This article has not been copyedited and formatted. The final version may differ from this version.

Fig 4

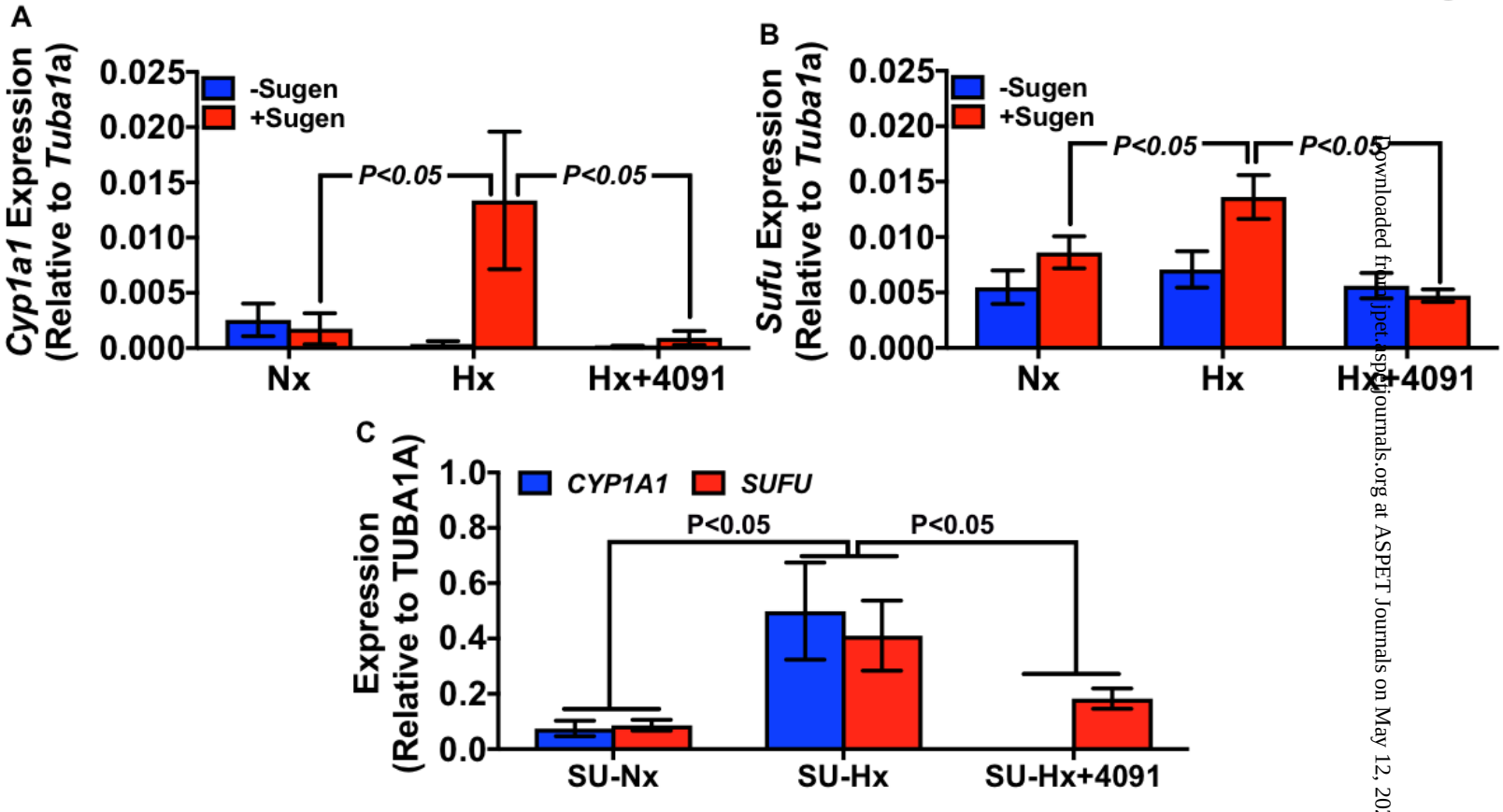

JPET Fast Forward. Published on March 23, 2021 as DOI: 10.1124/jpet.120.000166
This article has not been copyedited and formatted. The final version may differ from this version.

Fig 5